Characterization of the titanium Kβ spectral profile

C T Chantler[1], **L F Smale**[1], **J A Kimpton**[2], **D N Crosby**[3], **M N Kinnane**[1] **and A J Illig**[1]

[1] School of Physics, University of Melbourne, Parkville, 3010, Australia
[2] Australian Synchrotron, 800 Blackburn Road, Clayton, 3168, Australia
[3] Department of Physics, University of Oxford, Oxford, OX1-3PU, UK

E-mail: chantler@unimelb.edu.au

Abstract
Transition metals have Kα and Kβ characteristic radiation possessing complex asymmetric spectral profiles. Instrumental broadening normally encountered in x-ray experiments shifts features of profiles used for calibration, such as peak energy, by many times the quoted accuracies. We measure and characterize the titanium Kβ spectral profile. The peak energy of the titanium Kβ spectral profile is found to be 4931.966 ± 0.022 eV prior to instrumental broadening. This 4.5 ppm result decreases the uncertainty over the past literature by a factor of 2.6 and is 2.4 standard deviations from the previous standard. The spectrum is analysed and the resolution-free lineshape is extracted and listed for use in other experiments. We also incorporate improvement in analysis applied to earlier results for V Kβ.

S Online supplementary data available from stacks.iop.org/JPhysB/46/145601/mmedia

1. Introduction

High accuracy, absolute x-ray energy calibration is of great importance to making progress in x-ray science, including a better basis to test and develop QED and inner-shell process theory. Characteristic radiation (principally Kα and Kβ radiation) is often used as a calibration standard as the profiles are robust, stable and cheap to produce. The structure is properly modelled through the relativistic quantum theory of the atom, which has recently undergone significant development, especially for copper Kα [1]. Characterizations of the profiles permits new tests and understanding of atomic theory.

Excitation processes produce characteristic radiation including electron bombardment, x-ray absorption and inelastic x-ray scattering. These processes all involve an energetic incoming particle exciting the atom, and can be subject to sensitive chemical shifts and solid state effects. When the incoming particle has an energy just above threshold, the excited states and the shape of the characteristic energy profile sensitively depend upon the energy of the incoming particle [2, 3]. For electron bombardment, when the energy of the electron is at least 2.5 to 3 times the threshold energy of

the dominant transition, the excited state and profile shape of the characteristic radiation stabilize. This condition makes it possible to characterize the profile of Kβ radiation in a way that is robust to incoming electron energy variation. Standard x-ray sources include fixed anodes, rotating anodes, synchrotron excitation and others. We use a simple fixed source excitation following the standard technique of many past researchers. The question is, what is the stable profile which is thereby obtained, and how can it be robustly used, fitted and modelled in secondary and perhaps critical experiments?

A concerted effort to experimentally summarize experimental energies of characteristic radiation was undertaken and compiled by Bearden and Burr in 1967 [4]. This has been complemented by theoretical computations by Desclaux [5] as well as experimental measurement and compilation by Deslattes *et al* [6]. That review work summarized the peak energies of measured transitions without regard for the shifts and change of shape of the spectra due to experimental and instrumental broadening. Thus it is particularly difficult to compare advances in theory to results from high accuracy experiments. RMBPT has shown success with the inclusion of correlations to high-order and of the Auger shift. Quantum mechanics predict a shift and

Table 1. Characteristic radiation peak energy data from Chantler *et al* [19] and Deslattes *et al* [6]. The peak energy of the Kβ radiation has a larger uncertainty than for Kα radiation by an order of magnitude.

Spectral profile peak	Reference peak energy (eV)	Peak energy uncertainty (ppm)
Titanium Kα_1	4510.899 [6]	2.08
Titanium Kα_2	4504.920 [6]	2.09
Vanadium Kα_1	4952.131 [19]	1.21
Vanadium Kα_2	4944.651 [19]	2.22
Chromium Kα_1	5414.804 [6]	1.31
Chromium Kα_2	5405.538 [6]	1.31
Manganese Kα_1	5898.801 [6]	1.42
Manganese Kα_2	5887.685 [6]	1.43
Titanium Kβ_1	4931.83 [6]	12.0
Vanadium Kβ_1	5427.32 [6]	13.0

a broadening when a state is degenerate with a continuum [7, 8]. Significant advances in theory have been based on the relativistic approaches of Grant [9].

Experimental spectral profiles for the characteristic radiation of transition metals are represented by semi-empirical fitting of multiple components—using typically five or seven peaks for Kα spectra [10, 11]. Theoretical modelling of characteristic radiation profile shape is dominated by diagram line computations, which represent x-ray emission energies of electron decay from the ground state with a core-hole and an excited electron, to the ground state with the core-hole filled and a higher *n* hole. Additional components, theoretically and empirically, are contributed by satellite lines caused by shake-up and shake-off effects. This set of transitions is complex, especially for elements with open sub-shells such as the transition metals. Progress in the details of such theory has accelerated recently [12–15]. Empirical modelling using fitting functions for a sum of a small number of Lorentzian, Gaussian, Voigt or instrumental functions tends to conceal the theoretical complexity of the many CSF transitions.

Efforts to find good empirical models of spectral radiation have continued from the work of Deutsch *et al* and Hölzer *et al* of the 1990s [16, 10, 17, 11, 18]. Deslattes *et al* [6] includes a summary of these efforts, which is summarized with [19] in table 1 with experimental energies and uncertainties for Kα characteristic peaks for $Z = 22$–26. The uncertainties for the Kα energies in this range are on the order of 1 to 2 parts per million (ppm). However, the quoted uncertainty of the titanium Kβ peak energy [4] (table 1) is an order of magnitude larger at 12 ppm, limiting accuracy and calibration in this region of energy. In part, this is driven both by the weakness of Kβ compared to Kα, and the difficulty of calibration with suitable flux at low energies. In particular, although a nearby Kα spectrum can be used to calibrate some experiments, the Kβ adds a more critical and more difficult calibration affected by instrumental broadening but which is however less easily affected by vignetting. It therefore represents both a challenge and an opportunity for sharper and much more constrained calibration of accurate energies. We propose here and elsewhere to use a maximal calibration series including both Kα and Kβ characteristic lines. Other

methods are possible. However, until now, the accuracy of the determination of Kβ transitions generally precluded their utility for such purposes. This is the subject of the current paper.

Data collection methods generally use a single flat crystal spectrometer employing the Bond method [10, 11], or a curved crystal spectrometer [16]. In the experimental work arising from Germany [10, 11], raw spectra were deconvolved with a measured or fitted instrumental broadening, and each deconvolved spectrum was fit empirically with Lorentzians. The peak location of each empirical fit was taken to be the measure of each peak energy.

It is not immediately clear how to use these characterizations as standards for experiments with any different instrumental broadening. Chantler *et al* [19] addressed this concern by providing a consistent set of empirical Voigt fit functions for a range of elements ($21 \leqslant Z \leqslant 25$) including an approach to allow for instrumental broadening effects.

There has been some interest in the shape of the Ti Kβ profile over the years [20–24]. Much of this has been relating to efforts in calibration, as discussed above; but also because the characteristic signature provides valuable information about atomic structure, molecular and solid state effects including valence, ionization state, and Fermi levels in addition to electron correlations, excitation dynamics and relaxation processes. Interest has been raised in the identification of radiative Auger energies, KM$_1$ quadrupole decay, Kβ^{III} and Kβ^{IV} double ionization processes and other processes sometimes labelled Kβ' and Kβ_5. Additionally, x-ray astronomy has observed numerous K spectra of transition metals arising from plasmas of different types, and characterization of the profile can yield clues as to the nature of the plasma. This work has all been relative to the peak reported by Bearden and Burr [4], regarded as problematic in that the resolution and broadening shift was not calibrated.

A theoretical calculation of the peak energy for the diagram line of Ti Kβ is 4930.86(85) eV [6], consistent with the experimental result reported. However, the relatively high uncertainty in the Ti Kβ peak energy compared to those of Kα makes Ti Kβ a good candidate for improved characterization.

This paper presents the characterization of the titanium Kβ profile leading to a measurement of the energy of titanium Kβ peak energy after removal of instrumental broadening. The inclusion of broadening effects in the fitting method enables the results to be transferable to a large range of experimental conditions. Specifically, the characterization, or indeed the profile itself, can be simply used in experiments where the amount of instrumental broadening is difficult to measure.

2. Method of creation of the titanium Kβ standard profile

2.1. Experimental setup

A curved crystal spectrometer maps energy into position on a linear detector. The energy corresponding to each position along the detector is determined by measuring strong Kα

spectra, the peak values of which are known to $\simeq 1$ ppm from published measurements. This calibration is then used to place the Kβ spectrum on an energy scale. The measured spectrum is fitted by a sum of four Voigt functions with a common Gaussian width, representing the resolution function. Setting the Gaussian width to zero yields the 'intrinsic' resolution-smearing-free lineshape, the peak position of which may be taken as an instrument-independent Ti Kβ energy.

Experimental apparatus included a 20 keV electron bombardment x-ray source and a Johann geometry curved crystal spectrometer with position-sensitive x-ray detection. The apparatus was at the Oxford EBIT [25] as part of the calibration series for a test of QED. Figure 1 shows the arrangement of the calibration source, diffracting crystal, and detector. Significant details included the calibration anode, the Bragg angle of the arm that the detector sits on (2θ) an adjustable 'Seemann wedge' and a Germanium (220) crystal. The arm angle was fully adjustable with low hysteresis on the gearing and high reproducibility. The housing for the crystal is mechanically linked to the detector arm such that the crystal surface bisects the angle between the source and detector arm, so the crystal angle (θ) is half the arm angle. The crystal and arm angles are measured by gravity referenced electronic clinometers that output a raw voltage (V) which must be calibrated to clinometer angle I and then to θ. The Seemann wedge controls the band-pass of radiation through the crystal. One source of instrumental broadening is the gap between the wedge and the crystal surface. A multi-wire gas proportional counter with a backgammon configuration was used to detect x-rays, as well as provide good linearity and resolution in the dispersion axis.

For the calibration of the spectrometer, crystal alignment, and detector scale, a series of calibration spectra was collected in successive diffracting positions in order to assess systematics and evaluate the dispersion function. Table 1 provides the list of reference lines and their provenance, together with Kβ references for comparison. Clearly, the Kβ spectra currently provide poor reference lines compared to the Kα series or primary lattice spacing calibrations. The increased uncertainty is well-understood to be due to statistical precision and the Kβ intrinsic asymmetry—however, this paper explains how to realize determinations of the Kβ transitions with an accuracy approaching that of the Kα transitions.

2.2. Mosplate diffraction theory

The experimental process was modelled by the dynamical diffraction code, Mosplate [26, 27]. Mosplate predicts and models diffraction phenomena with effects on energy determination of 100–500 parts-per-million (ppm), and characterizes these with an accuracy and stability below 1 ppm. Diffraction phenomena of interest include the formal refractive index correction, but also crucial and independent dynamical diffraction depth penetration and geometric lateral shifts due to x-rays penetrating the crystal. Depth penetration of the dynamical wavefield can be a dominant systematic in curved crystal spectrometry but may be an even more significant effect in flat crystal spectrometry. Lateral shifts
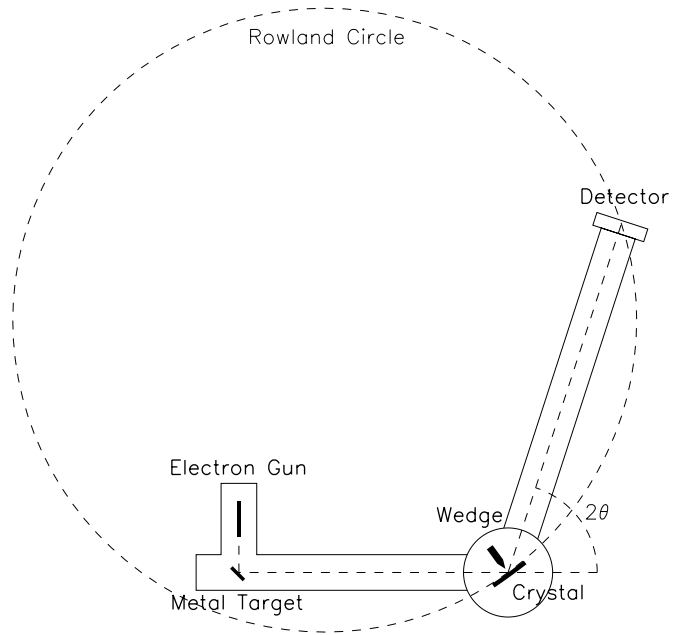

Figure 1. Schematic diagram of experimental setup.

can dominate in curved crystal spectrometry and are often a similar order of magnitude. Corrections for asymmetry and polarization are typically responsible for another 30 ppm. The refractive index shift, of order 100–200 ppm, is easily computed to high accuracy given knowledge of the (crystal) structure. However, the total or effective diffraction correction of 100–300 ppm, must be determined accurately to 1% or better. Figure 2 presents the effective refractive index based on the source location, size, crystal position and curvature, and detector location. The functional with respect to calibration lines is clear and stable, and more importantly the three curves presented reflect different detector–source positions (different Bragg angles to the axis of the crystal) which are set and characterized in the analysis. The associated uncertainty is of order 1.5 ppm, very similar to the uncertainty of the knowledge of the characteristic radiation energies. Figure 3 presents the similar effective shifts of the computed lines but including the changes of profile shape etc for one setting. The scale of the differential shifts and noise strongly support the final accuracy estimate of this uncertainty of 1.5 ppm.

For each x-ray energy E and crystal angle θ, Mosplate calculates the x-ray intensity spectrum we expect to see on the detector. The incident wavefield is computed by ray tracing performed from a point grid at the source to a point grid on the cylindrically curved crystal. The wavefield is then propagated through the crystal to find the diffracted wavefield at the exit surface of the crystal. The diffracted fields are then used as a source to ray trace to the final diffracted image on the detector. Once an appropriate range of single energy spectra is calculated at different crystal angles, a theoretical peak position, D, for each spectrum is computed.

These calculations of theoretical peak position sample the Mosplate model function for the peak position D and profile as a function of peak energy E and crystal angle θ:

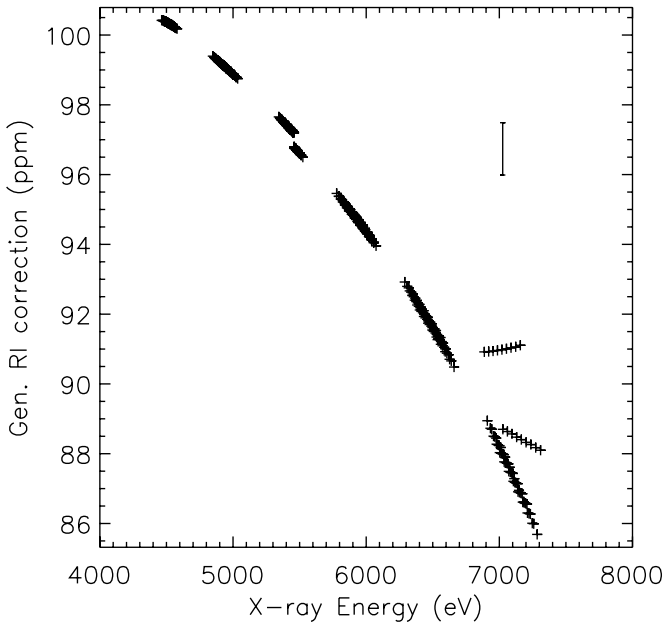$$D = D_{\mathrm{mos}}(E, \theta). \qquad (1)$$

Figure 2. This figure shows the effective refractive index correction given the specific geometry of the source, crystal and detector system. Note particularly (i) that the functional and convergence are well below the 1.5 ppm estimate (ii) the dispersion of the curves at higher energies is not uncertainty but predictive of the change in geometry depending upon the source-crystal axis angle. In other words, the variation is due to Mosplate correctly predicting the functional with position. Illustrated on the side is the estimated uncertainty of the characterization including input uncertainties, computed with a an approximately 1.5 ppm uncertainty error bar. This estimate would be substantively different with a flat crystal geometry.

This model also implicitly defines functions that calculate E and θ from the remaining variables:

$$E = E_{\mathrm{mos}}(D, \theta) \tag{2}$$

$$\theta = \theta_{\mathrm{mos}}(D, E). \tag{3}$$

These functions are interpolated between the sampling frequency of E and θ for which the results of $D_{\mathrm{mos}}(E, \theta)$ are computed to high accuracy. Interpolation uncertainty is negligible by design.

2.3. Data collection

Seven calibration series were conducted with a variety of wedge positions, offset positions of the detector, and integration times to interrogate systematics and confirm the accuracy of the theory. Data was collected in pseudo-event mode, so each x-ray is recorded as a separate pulse, rather than in an integrating detector. In each calibration series, Kα and Kβ spectral profiles from $Z = 22$–26 were collected. Each spectral profile type was collected at three to five detector arm angles, in order to investigate the dispersion function and the detector response function.

2.4. Kα profile modelling

The Kα profiles were fitted as functions of energy provided by [19]. Each of these functions are a sum of six Voigt profiles,
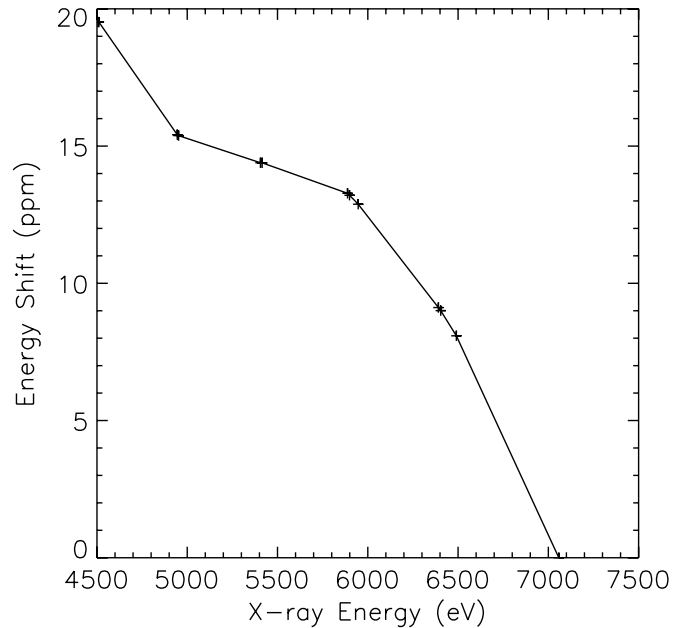

Figure 3. The energy shift from Bragg's law predicted by Mosplate, including peak and profile shifts as used in the computation, with an estimated uncertainty of 1.5 ppm.

with a common Gaussian width to model the instrumental broadening, which map x-ray energy to x-ray intensity. The energy offsets, Lorentzian widths, and relative amplitudes of the Voigt profiles are set by [19]. Each of the Kα experimental profiles were measured on a detector position axis rather than directly on an energy axis, so the profiles were fit by refining five fitting parameters: (i) a scale and (ii) an offset to map the detector position to energy, (iii) an intensity scale to model the overall intensity of the profile, (iv) a constant intensity background, and (v) a common Gaussian broadening width.

These highly accurate Kα characterizations provide a suite of peak energies correlated with the peak detector positions of each profile at each clinometer voltage. Figure 4 shows how one such fit leads to two calibration points.

2.5. Titanium Kβ profile fitting

Ti Kβ profiles were also collected and characterized on intensity and detector position axes. To define a characteristic lineshape function, each of the spectra were fitted using a sum of four Voigt functions with a common Gaussian width σ and a constant intensity background, B. Past literature has often used Lorentzians or Gaussians, which are generally inadequate. Profile decomposition can be made in principle with arbitrary functions. However, it is preferred that each component, even if semi-empirical in nature, should have a broadening representative of a real diagram line. The number of components is partially limited, or fixed, by the information content. It is obvious that at least three are required to produce the asymmetry. If three Voigts are attempted, there is a strong residual signature which is proof of the requirement for a fourth component. Equally, it is seen from table 2 that the area involved in the fourth peak is minor and that remaining residuals from figure 3 almost fully lie within the one standard
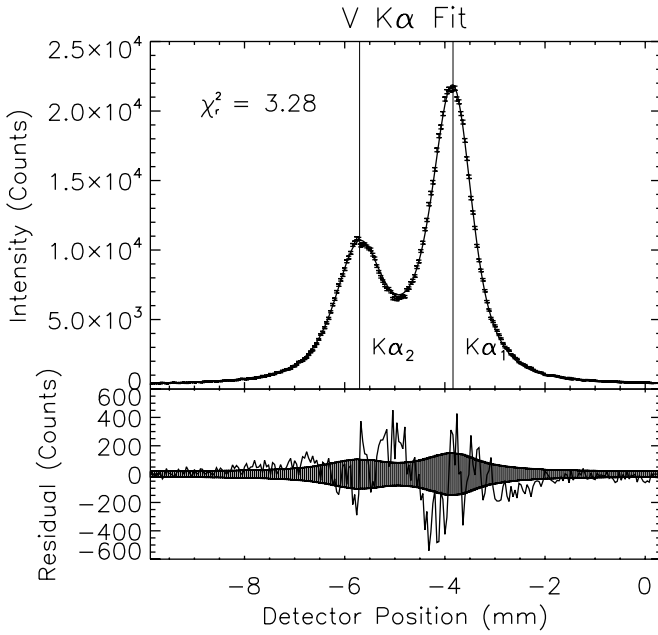
Figure 4. Typical fit of V Kα spectrum using only five scaling parameters, yielding two calibration points (V Kα$_1$ and V Kα$_2$ which constrain the spectrometer dispersion function). The fit has a χ_r^2 of 3.28. The Kα$_1$ peak has an energy 4952.131(6) eV and detector position $-3.8157(14)$ mm. The Kα$_2$ peak has an energy 4944.651(11) eV and detector position $-5.6973(26)$ mm. The crystal clinometer voltage was $-1.074\ 9865(99)$ V.

Table 2. Characterization of the Ti Kβ spectral profile. The profile is fully characterized on an absolute energy scale through a sum of component Lorentzians convolved with a Gaussian instrumental broadening. Integrated areas A_i, centroids C_i and FWHMs W_i of individual components were obtained from a fit of intensity against detector position. The detector position axis was transformed to an absolute energy scale via the calibration procedure. The Gaussian width $\sigma = 1.244(41)$ eV. The background was $B = 831(26)$ counts. The second and third components are dominant, contributing more than three quarters of the intensity of the spectrum while the fourth component is very weak. The third and fourth component widths are dominated by the Gaussian instrumental width. The first component is very broad relative to the entire Kβ spectrum.

Relative area $\frac{A_i}{\sum_{i=1}^{4} A_i}$	Integrated area A_i (counts)	Centroid C_i (eV)	FWHM W_i (eV)
0.199(24)	120 700(14 700)	4925.37(50)	16.3(10)
0.455(23)	276 000(13 700)	4930.096(75)	4.25(19)
0.326(22)	197 700(13 200)	4931.967(16)	0.42(22)
0.0192(54)	11 660(3250)	4935.59(16)	0.47(44)

error band. Hence there is no evidence for a fifth peak in the data itself.

The ith Voigt function used in the characterization is defined to be:

$$V(x; A_i, C_i, W_i, \sigma_i) = A_i \int_{-\infty}^{\infty} \left(\frac{e^{-x'^2/(2\sigma_i^2)}}{\sigma_i \sqrt{2\pi}} \right)$$
$$\times \frac{W_i/2}{\pi[(x - C_i - x')^2 + (W_i/2)^2]} \, dx' \quad (4)$$

where A_i is the integrated area of the Lorentzian profile, C_i is the centroid of the profile, W_i is the Lorentzian full width
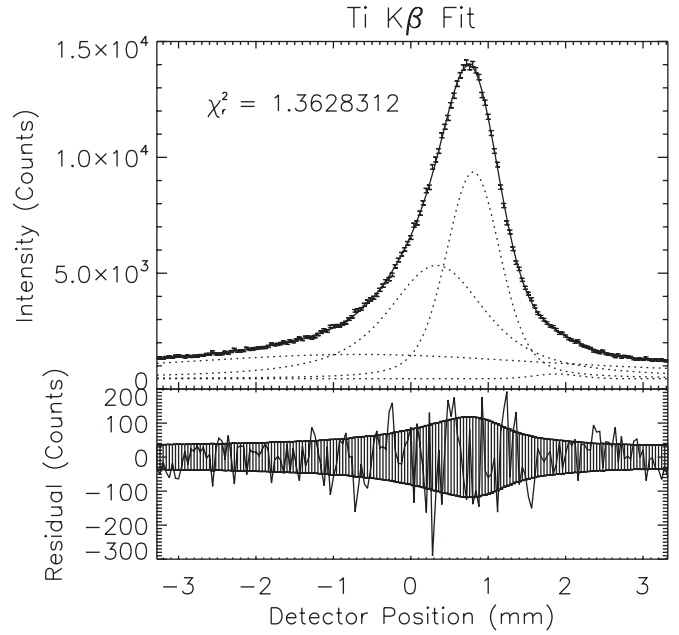

Figure 5. Typical fit of a Ti Kβ spectrum. The crystal clinometer voltage was $-1.012\ 9597(74)$ V and the peak detector position was 0.8089(14) mm. Fitting parameters are provided in table 2.

half maximum (FWHM) and σ_i is the Gaussian broadening standard deviation. The Gaussian broadening FWHM is $2\sqrt{2\ln 2}\sigma_i \approx 2.35\sigma_i$. Thus the spectra containing a Ti Kβ spectral profile were modelled with:

$$P(x; b, \sigma, A_1, C_1, W_1, A_2, C_2, W_2, A_3, C_3, W_3, A_4, C_4, W_4)$$
$$= B + \sum_{i=1}^{4} V(x; A_i, C_i, W_i, \sigma_i = \sigma). \quad (5)$$

A large collection of independent measurements of Ti Kβ profiles were fitted with this method. The relative intensities, positions and widths of the Voigt functions were consistent in all fits (to better than one standard error of the scaled fitting parameters), so the minimum uncertainty results are reported. The characteristic parameters of these fits are shown in table 2 with the position axis converted to energy. Figure 5 shows a typical fit for one of the Ti Kβ spectra.

These optimum parameters were then used to constrain refits of all the Ti Kβ profiles. Each refit had free parameters characterizing the overall intensity, position, detector position to energy scale conversion, instrumental broadening and background of the spectral profile in the specific geometry of the measurement. As each refit had a slightly different instrumental broadening due to geometry changes, the transferable reference position of the peak of each profile was the position of the maximum of the fit function with the Gaussian width set to zero. All refits were reliable and consistent with the original fits (to within one standard error of scaled parameter values); but the characterization allows for a consistent transferable standard both in this measurement, the calibration of the dispersion function, and for any subsequent measurement by other authors. This enabled a consistent measurement of peak position on any Ti Kβ profile for any local instrumental broadening.

2.6. Dispersion function for energy calibration

Two calibration functions are required to map the dispersion function and detector profile to an absolute energy axis. The clinometer calibration function $\theta = -I(V; P_I)$ maps the clinometer voltage V to the clinometer angle I and the dispersion crystal angle θ which reflects the theoretical Mosplate model crystal angle. $I(V; P_I)$ is defined to be:

$$I(V; P_I) = a\sin\left(\frac{V - P_{I,2}}{P_{I,0}}\right) - P_{I,1} + \sum_{i=0}^{n} P_{I,(i+3)}(V - P_{I,2})^i$$

(6)

where P_I is the vector of fitting parameters.

A second calibration function, the detector dispersion calibration function $D_2(x; P_D)$, maps the recorded detector position x in output units to the theoretical detector position D in mm. The map from x to D was defined by:

$$D_2(x; P_D) = \sum_{i=0}^{1} P_{D,i} x^i$$

(7)

where P_D is the vector of fitting parameters.

Using this calibration, an energy can be assigned for any detector position x and any clinometer voltage V:

$$E(x, V; P_D, P_I) = E_{\text{mos}}(D_2(x; P_D), -I(V; P_I)).$$

(8)

Equations (6) and (7) define the calibration of an experimental configuration (i.e. a calibration series). The calibration process was reduced to simultaneously finding the P_I and P_D fitting parameters that best fit the Kα data and produced an internally consistent measurement of the Ti Kβ peak energy for each calibration series. This optimized the statistical information for the determination of the profile and dispersion function. We use the evidence of the data to define a minimum-variance solution for parametrization of the dispersion function. In one sense this is a variant of a least-squares hypothesis, used widely in all statistical fitting but here we use it direcstly to assess the variance of the final measured energies.

2.7. Determination of energy uncertainty

Following equation (8), the uncertainty in the energy assigned to a detector position measurement, ΔE, was due to four primary sources of uncertainty: (i) detector position (Δx), (ii) detector dispersion fit $C_{D,ij}$, (iii) noise in clinometer voltage (ΔV), and (iv) clinometer calibration function fitting $C_{I,ij}$.

$$\Delta E^2 = \left(\frac{\partial E}{\partial x}\Delta x\right)^2 + \sum_{ij}\frac{\partial E}{\partial P_{D,i}}\frac{\partial E}{\partial P_{D,j}}C_{D,ij} + \left(\frac{\partial E}{\partial V}\Delta V\right)^2$$
$$+ \sum_{ij}\frac{\partial E}{\partial P_{I,i}}\frac{\partial E}{\partial P_{I,j}}C_{I,ij}$$

(9)

where $C_{D,ij}$ is the i,jth element of the covariance error matrix from the detector dispersion function fit. Likewise, $C_{I,ij}$ is the i,jth element of the covariance error matrix from the clinometer calibration function fit.

The clinometry calibration function covariance includes all uncertainties from clinometer nonlinearity, peak and energy uncertainty of Kα transitions and fitting, diffraction

Table 3. Error budget for the peak energy of all the spectral profiles of Ti Kβ that go into the final energy determination. Since the resultant determined energies show evidence of additional variance, the final energy determination has a larger uncertainty that this ideal 1.6 ppm for an individual spectrum.

Uncertainty source	Average contribution to energy uncertainty for an individual Ti Kβ spectrum (ppm)
Ti Kβ spectrum fit ($\frac{\partial E}{\partial x}\Delta x_{\text{fit}}$)	0.98
Detector dispersion function fit ($\sqrt{\sum_{ij}\frac{\partial E}{\partial P_{D,i}}\frac{\partial E}{\partial P_{D,j}}C_{D,ij}}$)	0.021
Clinometer noise ($\frac{\partial E}{\partial V}\Delta V$)	1.3
Clinometer calibration fit ($\sqrt{\sum_{ij}\frac{\partial E}{\partial P_{I,i}}\frac{\partial E}{\partial P_{I,j}}C_{I,ij}}$)	0.14
Total uncertainty	1.6

theory uncertainty and variance and other contributions. Kα peak position uncertainties are as detailed in table 1, and the uncertainties of the refractive index correction, dynamical diffraction modelling, geometric uncertainty and computational instability are approximately 1.5 ppm. These are included as input uncertainties of the $C_{I,ij}$ coefficients. Any temperature uncertainty cancels in the modelling (for this calibration methodology) because it produces an overall shift and not a relative shift of the spectra. The impact of uncertainty of the source position upon the diffraction computations is almost negligible. Further, the correlated uncertainty of more complex diffraction estimates cancels to first order. We detail the fitting procedure in the appendix. Table 3 shows the average magnitudes of these various contributions to ΔE outlined in section 2.7 for a single Ti Kβ spectrum.

3. Definition of titanium Kβ standard

3.1. Kβ peak energy

Fits of the Ti Kβ spectra provide independent measures of the peak energy of Ti Kβ, shown in figure 6. There is a systematic functional in the dispersion of measured energies with crystal angle. These data are pooled with their weighted mean reflecting the total uncertainty including the remanent systematic error.

The resulting measurement of the Ti Kβ profile peak energy is 4931.966(22) eV. This 4.5 ppm uncertainty is reduced from the larger uncertainty for individual fits given in table 3. Combining consistent samples in a weighted mean reduces uncertainty. We also computed the result after removing the two or three most significant outliers at the bottom of the graph, and the result changed insignificantly within sigma. The accuracy arises from the distribution of the results which are indeed clustered correctly about the centre of the detector. While the systematic could be asymmetric, we assume that it is symmetric and that our sampling measures this distribution. The previous theoretical reference value is 4930.86(85) eV [6]. The 1.106 eV or 1.3 standard deviation discrepancy from this is reflective of the claimed imprecision of the theoretical literature value.
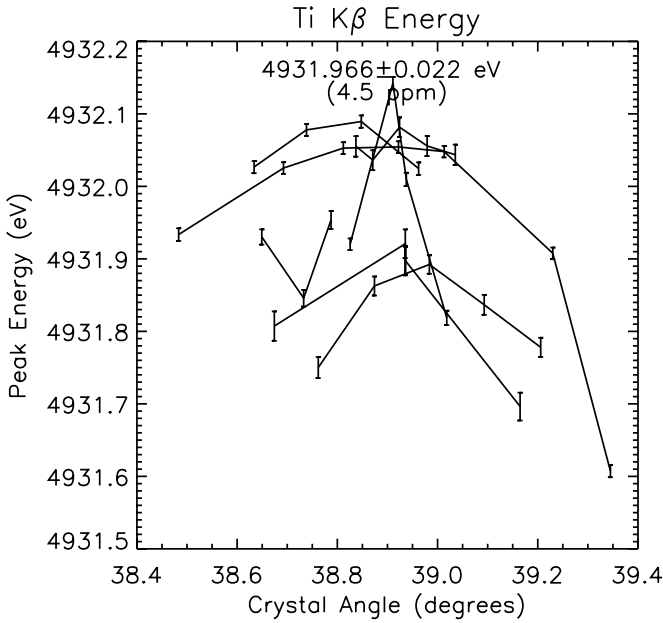
Figure 6. The peak energies of the fits of individual measured Ti Kβ spectra. Each of the seven lines represents an independently measured set of results from the full calibration series, derived by methodical stepping of the spectrometer arm length so that the profile stepped across the detector area. The variance is larger than the point precision, indicating sources of systematics. The characterization function drifts off towards the edges of the detector, where vignetting or other loss of efficiency may affect the calibration. Further, some of the linked series have offsets, whether from minor hysteresis or e.g. temperature variations. The overall consistency and hence robustness of the independent measurements yields a final pooled uncertainty of 4.5 ppm.

The new measurement represents a factor of 2.6 improvement in the uncertainty compared with the prior experimental value of 4931.827(59) eV, which had a 12 ppm uncertainty [4]. The discrepancy is 0.139 eV or about 2.4 standard deviations. Since an account of instrumental broadening is not given in the earlier experimental measurement, the 0.139 eV discrepancy is likely attributable to instrumental broadening. The relationship between peak energy and instrumental broadening is shown in figure 7. The asymmetry of the peak means that the greater the broadening, the more the peak energy is shifted to lower values. Hence any instrumental broadening will shift the peak energy significantly. We therefore present the instrumental-independent location and parameterization, so that it can be used with a general experimental methodology in situations with higher or lower resolution, in order to maintain an accurate calibration and energy transfer.

4. Use of the characterization of titanium Kβ

This paper offers a transferable characterization of Ti Kβ in terms of a sum of Voigt functions with a common instrumental (Gaussian) broadening, presented in table 2. This characterization functions as a standard reference for use in arbitrary experimental environments, where the instrumental broadening will be different. The instrumental broadening
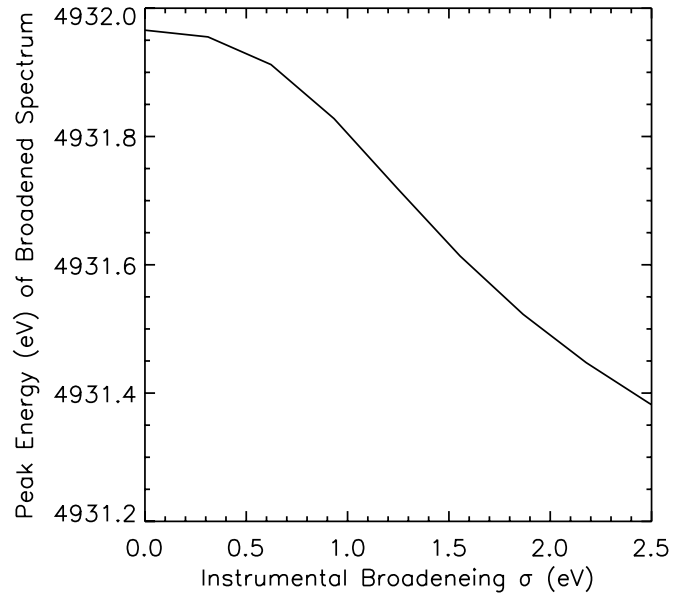

Figure 7. The peak energy of the fitted model function of the Ti Kβ spectra as a function of the instrumental broadening. The measured broadening of the spectrum of 1.24(4) eV and the asymmetry of the peak leads to a shift of peak position of 0.25 eV or 50 ppm.

should be fitted to the relevant profile, while the percentage contributions and eV widths of each component should remain unchanged. Fitting of an overall amplitude coefficient, the energy scale, and background to the experimental data should be all that is required to maintain the accuracy of the transfer. The simplest improvement over the previous literature is that a user may measure the Ti Kβ profile, remove the instrumental broadening, locate the peak position and then use the above determination to calibrate the spectrum.

A more accurate and transferable methodology would be to measure a Ti Kβ line as part of the calibration and then fit it with:

$$P_{\text{fit}}(X; B, \sigma, A, X_1, X_2) = P\left(X; B, \sigma, A, X_1, W_1 \frac{X_2 - X_1}{C_2 - C_1}, \frac{AA_2}{A_1},\right.$$

$$X_2, W_2 \frac{X_2 - X_1}{C_2 - C_1},$$

$$\frac{AA_3}{A_1}, (C_3 - C_1) \frac{X_2 - X_1}{C_2 - C_1} + X_1, W_3 \frac{X_2 - X_1}{C_2 - C_1},$$

$$\left.\frac{AA_4}{A_1}, (C_4 - C_1) \frac{X_2 - X_1}{C_2 - C_1} + X_1, W_4 \frac{X_2 - X_1}{C_2 - C_1}\right) \quad (10)$$

where the A_is, C_is and W_is come from table 2, the X_i parameters are the positions of the first 2 Voigt peaks, A is the area of the first peak, σ is the Gaussian width of all the Voigt profile components and B is the background height. This characterization of Ti Kβ can be directly transferred to other experiments to generate calibration points for high accuracy x-ray experiments.

An alternative methodology would be to use the directly measured and calibrated profile attached to this paper as supplementary material (ti_deposition.txt)(available from stacks.iop.org/JPhysB/46/145601/mmedia), though with correction for any broadening from the instrumental function. Use this directly, fitting only the amplitude, detector scale and background to yield an accurate and transferable standard.
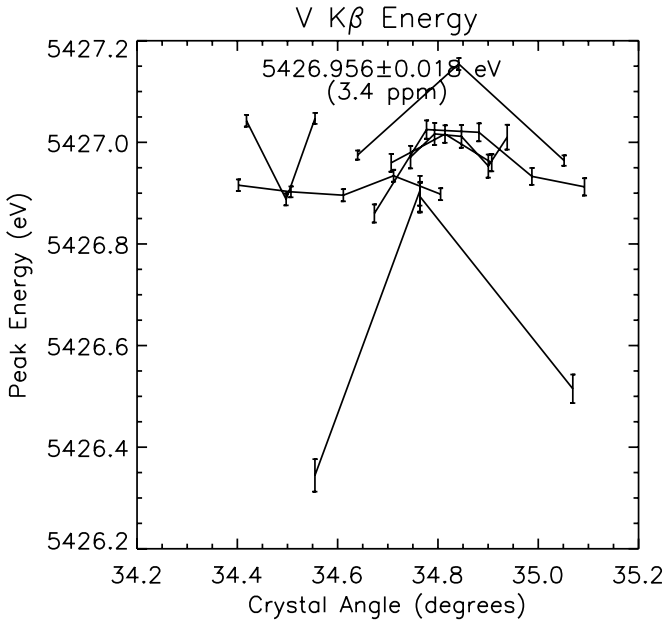
Figure 8. The peak energies of the fits of individual measured V Kβ spectra. Each of the seven lines represents an independently measured set of results from the full calibration series, derived by methodical stepping of the spectrometer arm length so that the profile stepped across the detector area. The variance is larger than the point precision, indicating sources of systematics. The characterization function drifts off towards the edges of the detector, where vignetting or other loss of efficiency may affect the calibration. Further, some of the linked series have offsets, whether from minor hysteresis or e.g. temperature variations. The overall consistency and hence robustness of the independent measurements yields a final pooled uncertainty of 0.0184 eV or 3.4 ppm.

Table 4. The full characterization of the V Kβ spectral profile on an absolute energy scale. The parameters in this table are used in equation (5). Amplitudes A_i, centroids C_i and widths W_i of individual components were obtained from a fit on the intensity versus detector position axis. The detector position axis was transformed to an absolute energy scale via the calibration procedure. The Gaussian width σ was 0.805(25) eV. The background was 749(24) counts.

Proportion of area $\frac{A_i}{\sum_{i=1}^4 A_i}$	Integrated area A_i (counts)	Centroid C_i (eV)	Width W_i (eV)
0.258(21)	160 000(13 000)	5418.19(35)	18.86(83)
0.236(18)	147 000(11 000)	5424.50(11)	5.48(21)
0.507(14)	315 300(8500)	5426.992(13)	2.499(69)

5. Redefinition of vanadium Kβ standard

A definition of a vanadium Kβ standard was reported by the present authors in [28]. The calibration in that paper relied on fits of narrower (less robust) ranges of the Kα spectra in section 2.4 and neglected propagating the uncertainty from the diffraction theory of Mosplate added to the calibration fitting. This previous result yielded a definition of the vanadium Kβ profile peak energy of 5426.962(15) eV. Applying the modified methods in this paper results in a characterization of the V Kβ profile presented in table 4. The peak energy was found to be 5426.956(18) eV as shown in figure 8. This represents a shift of 0.006 eV (0.4 of a standard error). The small shift shows

that the two results are consistent with each other as expected, and that the earlier characterization was in fact robust within stated uncertainty.

6. Conclusion

The spectral profile of Ti Kβ was measured and characterized in a transferable methodology. The characterization involved modelling the profile with four Lorentzian peaks convolved with an overall Gaussian. The Gaussian is recommended to model additional (instrumental) broadening, so long as significant profile vignetting is not involved—that is, so long as the profiles are complete Kβ profiles and not truncated by the source size or slit width. In fact, this method reveals the significance of any such vignetting by returning a high χ_r^2 value for the fits, and by being strongly dependent on crystal or diffracting angle with a clear asymmetry of the fit. The individual widths for each Lorentzian component are described and tabulated. The Ti Kβ peak energy was found to be 4931.966(22) eV. This is an improvement in uncertainty by a factor of 2.6 over the previous best reported result. It must be remembered that the previous tabulated value had not resolved the issue of instrumental broadening as a significant source of peak shift. We have deposited the full profile for use by advanced researchers or for direct comparison with a calibration profile without the parametric modelling. We recommend that the component modelling is reliable and much more accurate than previous approaches and is a recommended standard methodology for future x-ray calibration. The V Kβ profile characterization was also updated with a new methodology and found to be consistent within uncertainty of the prior analysis.

Appendix. Dispersion function and detector position

Fitting parameters P_I and P_D for each calibration were determined following four major steps: clinometer pre-calibration; clinometer calibration first estimate; calibration fitting; and detector scale correction. Preliminary clinometer pre-calibration entailed an experimental characterization of the angle of incline to voltage function ($V_{\text{pre}}(I)$) of the clinometers in isolation:

$$V_{\text{pre}}(I) = P_{V,0} \sin(I - P_{V,1}) - P_{V,2} + \sum_{i=0}^{8} P_{V,(i+3)} V^i. \quad \text{(A.1)}$$

Second, an estimate of the clinometer calibration function was constructed by generating data with the $V_{\text{pre}}(I)$ function, inverting the data, and then fitting this data with $I(V; P_I)$ (equation (6)) where a third order polynomial was found to be adequate.

Third, calibration fitting was a six stage process beginning with estimation of P_I and P_D (figure A1). Each stage made a refinement of either P_I or P_D through one round of refitting. At the end of this step, the fitted P_I parameters reflected the measured clinometer functionals. The six stage calibration fitting used the interlinked Kα reference peak energy, detector peak position and clinometer voltage calibration data to robustly determine the dispersion function, with a set of Kα
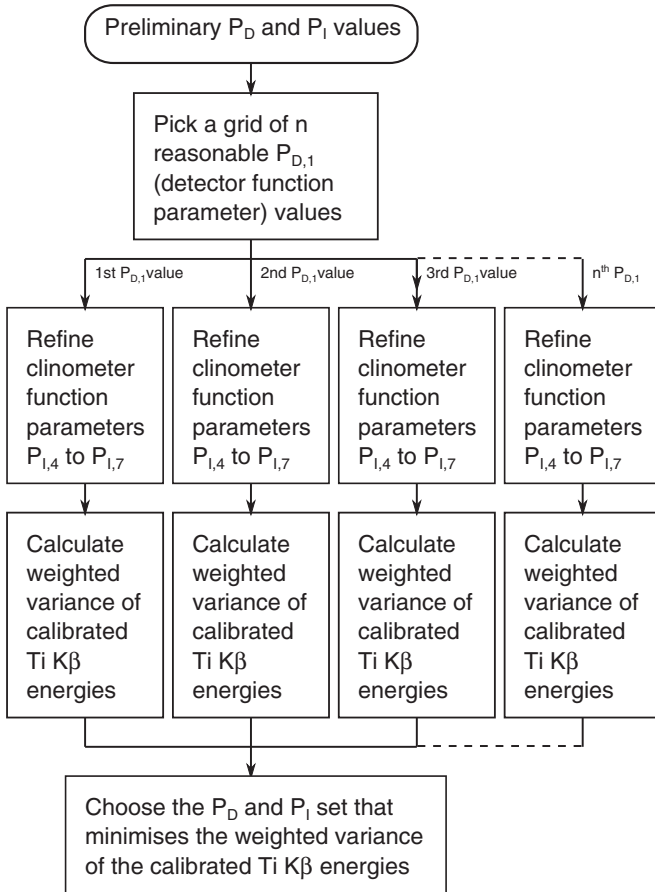
Figure A1. Refitting process schematic.

measurements defining the robustness and consistency of the determination. Prior to each fitting, this data was processed to produce one of two axis sets, I_{data} or D_{data}.

Axis set 1 fitted I_{data} versus V where I_{data} is the set of calculated data providing the expected clinometer angle for each peak based on the energy and detector position.

$$I_{\text{data}} = -\theta_{\text{mos}}(D_2(x, P_D), E). \qquad (A.2)$$

It has uncertainty ΔI_{data}:

$$\Delta I_{\text{data}}^2 = \left(\frac{\partial \theta_{\text{mos}}}{\partial E}\Delta E\right)^2 + \left(\frac{\partial \theta_{\text{mos}}}{\partial D}\right)^2\left(\sum_{ij}\frac{\partial D}{\partial P_{D,i}}\frac{\partial D}{\partial P_{D,j}}C_{D,ij}\right.$$
$$\left. + \left(\frac{\partial D}{\partial x}\Delta x\right)^2\right). \qquad (A.3)$$

Axis set 2 fitted D_{data} versus x where D_{data} is the set of calculated data providing the expected theoretical detector position for each peak based on the energy and crystal angle.

$$D_{\text{data}} = D_{\text{mos}}(E, -I(V; P_I)). \qquad (A.4)$$

It has uncertainty ΔD_{data}:

$$\Delta D_{\text{data}}^2 = \left(\frac{\partial D_{\text{mos}}}{\partial E}\Delta E\right)^2 + \left(\frac{\partial D_{\text{mos}}}{\partial \theta}\right)^2\left(\sum_{ij}\frac{\partial I}{\partial P_{I,i}}\frac{\partial I}{\partial P_{I,j}}C_{I,ij}\right.$$
$$\left. + \left(\frac{\partial I}{\partial V}\Delta V\right)^2\right) \qquad (A.5)$$

The first fit of axis set 1 was calculated using the estimated P_D parameters with $I(V; P_I)$ and only allows the refinement of $P_{I,1}$. The second step was a refit of axis set 1 with $I(V; P_I)$ using the P_I from fit 1 as a estimate, this time only allowing the refinement of $P_{I,4}$ through $P_{I,7}$, fitting the fine details and secondary functional parameters of $I(V; P_I)$. The third fit was of axis set 2, calculated using the refined P_I parameters from the second fit, using $D(x; P_D)$. Fourthly, results from this third step were then used to refit axis set 1 and $I(V; P_I)$ allowing the refinement of $P_{I,4}$ through $P_{I,7}$, as in the second fit. Fits five and six are a repeat of the third and fourth fits using the output of fit four as the input of fit five. This method generates the P_I and P_D parameters along with associated covariance error matrices C_I from the sixth fit and C_D from the fifth fit.

Finally, a detector scale refinement investigated the value of $P_{D,1}$ (the detector scale) by grid search to minimize the uncertainty and variance of the weighted mean of the peak energy of all Ti Kβ spectra. A low uncertainty (variance) in the weighted mean represents greater consistency between independent spectra. For each $P_{D,1}$ value in the grid search there was a three step process: (1) a fit of axis set 1 to refine the clinometer calibration function in the context of that detector scale; (2) modelling of the Ti Kβ peak position and a clinometer voltage data for all of the calibration series using equation (8) to generate a set of Ti Kβ peak energies and uncertainties for the calibration series; (3) computing the weighted mean and corresponding uncertainty from the variance of the set of energies. The final calibration was then represented by the refined fitting parameters which reflect the experimental minimization of systematic variance around Ti Kβ. For clarity, we provide a schematic summarizing the refinement process (figure A1).

References

[1] Chantler C T, Lowe J A and Grant I P 2010 Multiconfiguration Dirac–Fock calculations in open-shell atoms: convergence methods and satellite spectra of the copper Kα photoemission spectrum *Phys. Rev.* A **82** 052505
[2] Fritsch M, Kao C C, Hämäläinen K, Gang O, Förster E and Deutsch M 1998 Evolution of the Cu K$\alpha_{3,4}$ satellites from threshold to saturation *Phys. Rev.* A **57** 1686
[3] Deutsch M, Gang O, Hämäläinen K and Kao C C 1996 Onset and near threshold evolution of the Cu Kα x-ray satellites *Phys. Rev. Lett.* **76** 2424–7
[4] Bearden J A and Burr A F 1967 Reevaluation of x-ray atomic energy levels *Rev. Mod. Phys.* **39** 125–42
[5] Desclaux J P 1973 *At. Data Nucl. Data Tables* **12** 312
[6] Deslattes R D, Kessler E G, Indelicato P, de Billy L, Lindroth E and Anton J 2003 X-ray transition energies: new approach to a comprehensive evaluation *Rev. Mod. Phys.* **75** 35–99
[7] Indelicato P, Boucard S and Lindroth E 1998 Relativistic and many-body effects in K, L, and M shell ionization energy for elements with and the determination of the 1s lamb shift for heavy elements *Eur. Phys. J.* D **3** 29–41
[8] Mooney T, Lindroth E, Indelicato P, Kessler E G Jr and Deslattes R D 1992 Precision measurements of K and L transitions in xenon: experiment and theory for the K, L, and M levels *Phys. Rev.* A **45** 1531
[9] Grant I P 1970 *Adv. Phys.* **19** 747

[10] Deutsch M, Hölzer G, Härtwig J, Wolf J, Fritsch M and Förster E 1995 Kα and Kβ x-ray emission spectra of copper *Phys. Rev.* A **51** 283–96
[11] Hölzer G, Fritsch M, Deutsch M, Härtwig J and Förster E 1997 Kα$_{1,2}$ and Kβ$_{1,3}$ x-ray emission lines of the 3d transition metals *Phys. Rev.* A **56** 4554–68
[12] Chantler C T, Hayward A C L and Grant I P 2009 Theoretical determination of characteristic x-ray lines and the copper Kα spectrum *Phys. Rev. Lett.* **103** 123002
[13] Lowe J A, Chantler C T and Grant I P 2010 A new approach to relativistic multi-configuration quantum mechanics in titanium *Phys. Lett.* A **374** 4756–60
[14] Chantler C T, Lowe J A and Grant I P 2010 Multiconfiguration Dirac–Fock calculations in open shell atoms: convergence methods and satellite spectra of copper Kα photoemission spectrum *Phys. Rev.* A **82** 052505
[15] Lowe J A, Chantler C T and Grant I P 2011 *Ab initio* determination of satellite intensities in transition-metal photoemission spectroscopy using a multiconfiguration framework *Phys. Rev.* A **83** 060501
[16] Anagnostopoulos D F, Sharon R, Gotta D and Deutsch M 1999 Kα and Kβ x-ray emission spectra of metallic scandium *Phys. Rev.* A **60** 2018–33
[17] Anagnostopoulos D F, Gotta D, Indelicato P and Simons L M 2003 Low-energy x-ray standards from hydrogenlike pionic atoms *Phys. Rev. Lett.* **91** 240801
[18] Schweppe J, Deslattes R D, Mooney T and Powell C J 1994 Accurate measurement of Mg and Al Kα$_{1,2}$ x-ray energy profiles *J. Electron. Spectrosc. Relat. Phenom.* **67** 463–78
[19] Chantler C T, Kinnane M N, Su C-H and Kimpton J A 2006 Characterization of Kα spectral profiles for vanadium,

component redetermination for scandium, titanium, chromium, and manganese, and development of satellite structure for $Z = 21$ to $Z = 25$ *Phys. Rev.* A **73** 012508
[20] Limandri S P, Carreras A C, Bonetto R D and Trincavelli J C 2010 Kβ satellite and forbidden transitions in elements with $12 \leqslant Z \leqslant 30$ induced by electron impact *Phys. Rev.* A **81** 012504
[21] Koster A S and Mendel H 1970 X-ray Kβ emission spectra and energy levels of compounds of 3D-transition metals—I: oxides *J. Phys. Chem. Solids* **31** 2511–22
[22] Uršič M, Kavčič M and Budnar M 2003 Second order radiative contributions in the Kβ$_{1,3}$ x-ray spectra of 3d transition metals and their dependence on the chemical state of the element *Nucl. Instrum. Methods Phys. Res.* B **211** 7–14
[23] Morita S and Fujita J 1985 Kβ x-ray transition energies of M-shell-ionized ions of Ti through Ni in a plasma *Phys. Rev.* A **31** 3299
[24] Mandić L, Fazinić S and Jakšić M 2009 Chemical effects on the Kβ and Kβ$_{2,5}$ x-ray lines of titanium and its compounds *Phys. Rev.* A **80** 042519
[25] Silver J D *et al* 1994 The Oxford electron-beam ion trap: a device for spectroscopy of highly charged ions *Rev. Sci. Instrum.* **65** 1072–4
[26] Chantler C T 1992 X-ray diffraction of bent crystals in Bragg geometry: I. Perfect-crystal modelling *J. Appl. Crystallogr.* **25** 674–93
[27] Chantler C T 1992 X-ray diffraction of bent crystals in Bragg geometry: II. Non-ideally imperfect crystals, modelling and results *J. Appl. Crystallogr.* **25** 694–713
[28] Smale L F, Chantler C T, Kinnane M N, Kimpton J A and Crosby D N 2013 Characterization of the Kβ spectral profile for vanadium *Phys. Rev.* A **87** 022512